Multimaterial 3D printing of auxetic jounce bumpers for automotive suspensions

Multimaterial 3D printing of auxetic jounce bumpers for automotive suspensions

Alberto Giubilini and Paolo Minetola
Departement of Management and Production Engineering, Politecnico di Torino, Turin, Italy

Abstract

Purpose – The purpose of this study is to evaluate the 3D printability of a multimaterial, fully self-supporting auxetic structure. This will contribute to expanding the application of additive manufacturing (AM) to new products, such as automotive suspensions.

Design/methodology/approach – An experimental approach for sample fabrication on a multiextruder 3D printer and characterization by compression testing was conducted along with numerical simulations, which were used to support the design of different auxetic configurations for the jounce bumper.

Findings – The effect of stacking different auxetic cell modules was discussed, and the findings demonstrated that a one-piece printed structure has a better performance than one composed of multiple single modules stacked on top of each other.

Research limitations/implications – The quality of the 3D printing process affected the performance of the final components and reproducibility of the results. Therefore, researchers are encouraged to further study component fabrication optimization to achieve a more reliable process.

Practical implications – This research work can help improve the manufacturing and functionality of a critical element of automotive suspension systems, such as the jounce bumper, which can efficiently reduce noise, vibration and harshness by absorbing impact energy.

Originality/value – In previous research, auxetic structures for the application of jounce bumpers have already been suggested. However, to the best of the authors' knowledge, in this work, an AM approach was used for the first time to fabricate multimaterial auxetic structures, not only by co-printing a flexible thermoplastic polymer with a stiffer one but also by continuously extruding multilevel structures of auxetic cell modules.

Keywords Additive manufacturing (AM), Auxetic structures, Jounce bumpers, Fused filament fabrication (FFF)

Paper type Research paper

1. Introduction

In automotive suspension systems, a key role is played by the jounce bumper, which is typically mounted between the damper and base of the shock absorber and is surrounded by a suspension spring. Its essential function is to absorb impact energy, avoiding a complete compression of the suspension component, thus resulting in an improvement in the noise, vibration and harshness (NVH) performance (Wang *et al.*, 2018a, 2018b, 2018c). The jounce bumper can also function as an auxiliary spring when the main spring is close to its maximum load (Wang *et al.*, 2018a, 2018b, 2018c). Generally, jounce bumpers are made of materials with hyperelastic properties, such as rubber or polyurethane (PUR), which are suitable for enhancing comfort while driving (Wang *et al.*, 2016a, 2016b). Basic mechanical characterization of the jounce bumpers is achieved through compression tests. The optimal condition is represented when the load–displacement curve is contained within an ideal region, defined by a lower and upper limit. This region is determined by optimizing the NVH performance of the car (Wang *et al.*, 2016a, 2016b). Another possible and interesting characterization of these devices is the evaluation of their fatigue life, owing to the continuous and cyclic state of loading and unloading they are subjected to, to avoid a sudden failure by fatigue.

Previous studies conducted by Wang *et al.* suggested using innovative structures with enhanced mechanical performance in terms of fracture resistance and shear modulus (Jiang and Li, 2017) to replace traditional jounce bumpers. One of the most promising solutions is to use auxetic geometries (Wang *et al.*, 2017; Wang *et al.*, 2016a, 2016b; Wang *et al.*, 2018a, 2018b, 2018c; Wang *et al.*, 2018a, 2018b, 2018c). The analyses proposed experimental and numerical simulations of negative Poisson's ratio (NPR) architectures, compressed by a uniaxial load. By definition, materials or structures with auxetic properties have the characteristic of presenting a negative Poisson's ratio, which for uniaxial stress is expressed as:

$$\upsilon_{ij} = -\frac{\varepsilon_j}{\varepsilon_i}$$

The authors gratefully acknowledge Mr Davide Finotto for his help in the design and production of the auxetic structures. Mention should also be made to Mr Aresh Mazdai who contributed to the first draft of the paper.

Received 20 February 2023
Revised 12 July 2023
22 September 2023
Accepted 23 September 2023

The current issue and full text archive of this journal is available on Emerald Insight at: **https://www.emerald.com/insight/1355-2546.htm**

Rapid Prototyping Journal
29/11 (2023) 131–142
Emerald Publishing Limited [ISSN 1355-2546]
[DOI 10.1108/RPJ-02-2023-0066]

Figure 1 Tensile behavior for non-auxetic material (a) and auxetic material (b)

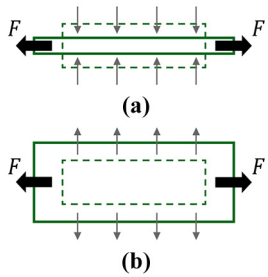

Source: Figure by authors

where v_{ij} is Poisson's ratio (PR), ε_j is the transverse strain and ε_i is the axial strain.

The PR is an indication of the volume variation in tensile or compression deformations [Figure 1(a)], and the physical interpretation of a NPR reflects lateral expansion during tension and lateral shrinkage under compression [Figure 1(b)].

Therefore, compared to traditional jounce bumpers, the specific advantage of these new architectures lies in the possibility of the NPR geometries shrinking laterally under compression, thereby enhancing the stiffness of the entire structure. This increased mechanical response may have some interesting secondary advantages. For example, there is the possibility of reducing the amount of material expected for the same property requirements, as well as the chance to remove the cup and reinforcement rings from the suspension assembly (Wang *et al.*, 2016a, 2016b). Auxetic behavior occurs in both natural and synthetic structures. Examples of the former are arsenic and cadmium monocrystals, polymorphous α-cristobalite of crystalline silica, zeolites and graphite used in nuclear reactors (Baughman *et al.*, 1997; Baughman and Galvão, 1993; Friis *et al.*, 1988; Wojciechowski, 1987). Many artificial auxetic materials were investigated in the last 20 years (Jiang *et al.*, 2022), for example, PUR foam (Alderson and Alderson, 2007), microporous poly (tetrafluoroethylene) (Alderson *et al.*, 2002) and microporous ultra-high molecular weight polyethylene (Herakovich, 1984).

In recent years, with the growing importance and development of additive manufacturing (AM) techniques, research has focused on the design and the fabrication of auxetic structures with intricate cellular architectures via 3D printing (Hedayati *et al.*, 2021; Meena and Singamneni, 2021; Meena *et al.*, 2023). Unlike traditional manufacturing, AM makes complex geometries viable with much higher freedom in design for final shapes that cannot otherwise be achieved (Joseph *et al.*, 2023). Zhang et *al.* proposed an interesting and comprehensive review of the most recent progress in the field of additively manufactured auxetic structures and compared and summarized the results of mechanical properties under quasi-static and dynamic loading, energy absorption and numerical simulations of different geometries (Zhang *et al.*, 2020). Moreover, it was demonstrated that by varying the internal geometric morphology of the structures, it is possible to tune their final mechanical properties, such as the elastic modulus, damage mode, peak force and energy absorption (Guo *et al.*, 2021). Using the most recent AM techniques, it was also possible to design a single structure with a nonuniform distribution of auxetic cells, that is, a geometry with tunable PR and variable deformation properties, built by connecting different elementary cells with different PR (Han and Lu, 2018). In their latest work, Hu *et al.* raised a point of considerable interest concerning the 3D printing of a structure that can be self-standing and that does not require any kind of support material to simplify and speed up the fabrication process. The authors proposed a 3D-repeating tetrahedron framework with concave points oriented obliquely downward so that the structure can be 3D printed without supports (Hu *et al.*, 2022).

Even recently published studies (Chapa *et al.*, 2023; Ramírez-Gutiérrez *et al.*, 2023), which use fused filament fabrication (FFF) technology to produce auxetic components, have exploited the simple repetition of the same geometry layer after layer, keeping the deposition path constant for each successive layer.

Conversely, this research work is a preliminary study to evaluate the printability via AM of a multimaterial auxetic component that is completely self-supporting with a printing direction that enables the design of a closed-loop circular arrangement of single auxetic cells. FFF technology was exploited to produce NPR components, which may have possible future applications in automotive suspension assembly, as illustrated in Figure 2. This AM technology offers the possibility of realizing complex geometries and combining different materials into a single structure using a 3D printer with multiple extruders. Because of the many variables affecting the behavior of jounce bumpers and the complexity of their design (Wang *et al.*, 2016a, 2016b), this study starts with the definition of the geometry of a simple auxetic cell that can be 3D printed without supports. The resulting geometry was first prototyped, and then the cell was replicated to create modules for the jounce bumper. The compression behavior of different types of modules was characterized by load–displacement tests using experimental and numerical methods.

2. Design and production of multimaterial auxetic jounce bumpers

2.1 Design of the elementary negative Poisson's ratio cell

To determine a suitable auxetic structure to be fabricated by AM, a honeycomb cell with reentrant sides (Lu *et al.*, 2016),

Figure 2 Rendering of an automotive suspension with the application of the 3D printed auxetic jounce bumper in green

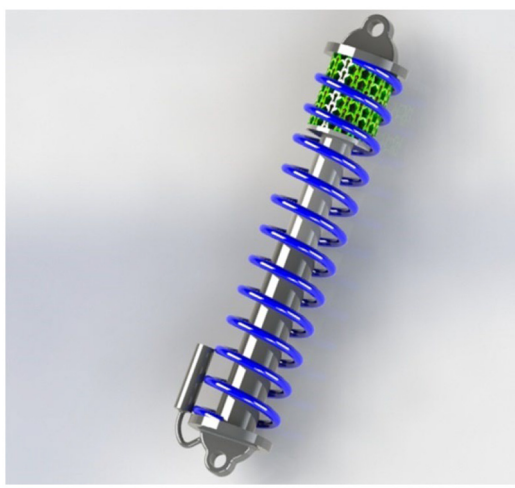

Source: Figure by authors

Figure 3 The analytical model of a reentrant auxetic structure (a); 3D printed reentrant auxetic prototype (b)

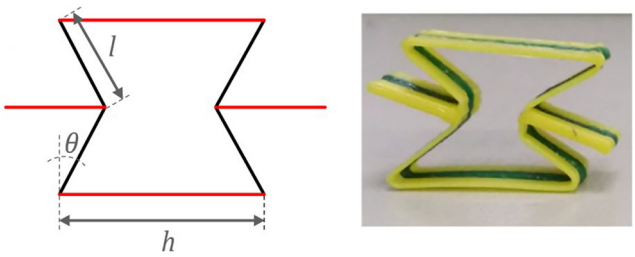

(a) (b)

Source: Figure by authors

which is one of the earliest NPR geometries proposed in the literature, was considered [Figure 3(a)]. First, a 3D model of the cell was printed from poly(lactic acid) (PLA, yellow) and thermoplastic polyurethane (TPU, green) with the following dimensions: $h = 20$ mm, $l = 10$ mm and $\theta = 10°$. The combination of the two materials was defined as a sandwich structure, in which the TPU material was placed between the PLA material [Figure 3(b)]. To this end, 15 layers of flexible TPU material were interposed with 15 top and 15 bottom layers of rigid PLA in the building direction, using a layer thickness of 0.2 mm. Figure 3(b) shows a single reentrant cell, where the outer perimeter of the geometry in Figure 3(a) was 3D printed using the sandwich structure strategy described above.

This printing orientation was selected to avoid the use of support structures. The possibility of avoiding support structures can significantly reduce the amount of material required; therefore, the manufacturing process is faster, simpler, and more environmentally friendly. However, when designing a 3D structure with auxetic cells in a ring arrangement, it was necessary to modify the original cell geometry [Figure 3(a)] and also change its printing direction to make it self-supporting. To achieve a ring-shaped 3D printed module consisting of several auxetic cells, the growth direction of the 3D print was changed, starting from the bottom cell and then reaching the top layer-by-layer. Moreover, to create a self-supporting geometry, the original geometry was modified by tilting the four horizontal sides of the cell by 45° [Figure 4(a)]. The changes to the single elements of the auxetic cell are highlighted in red in Figure 4(b), where PLA was used to impart stiffness to the system, and it was placed in the inner core of the structure, near the central

Figure 4 Improved cell design with combination of TPU and PLA materials (a); the modification of the cell geometry suggested by the authors (b)

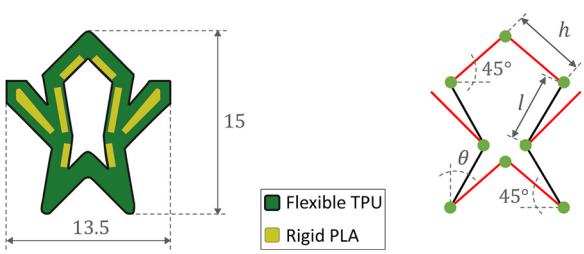

(a) (b)

Source: Figure by authors

opening, and in the core of the side wings [yellow areas in Figure 4(a)]. In contrast, the TPU envelope was created to wrap the entire cell geometry [green area in Figure 4(a)] and provide flexibility, especially in the junctions [green dots in Figure 4(b)]. In this preliminary work, no calculations or simulations were conducted considering the size of the PLA inserts and the influence of the resulting number of 3D printing layers, which are better visible in Figure 10(a). In the modification of the auxetic cell, PLA inserts were just encapsulated in the TPU envelope to promote and ensure good adhesion between the two materials while preserving the flexibility in the junctions. Moreover, considering the small size of the cell, there is little opportunity to further increase the length of the PLA inserts [Figure 10(a)], which might be shortened to increase the flexibility.

2.2 Design and numerical simulation of innovative negative Poisson's ratio configurations

After defining the innovative cell geometry for 3D printing, the overall structure of auxetic jounce bumpers was designed and simulated to obtain a proper understanding of the compression behavior of these devices. To this end, two different configurations were developed to evaluate the effect of inclination θ of the reentrant sides on the auxetic properties at an angle of 5° (configuration 1) or 15° (configuration 2). For both configurations, a wall thickness of 1 mm was selected, and h and l dimensions [Figure 4(b)] were set at 6 mm and 5.5 mm, respectively.

The auxetic behavior of the two innovative configurations was evaluated by a finite element method (FEM) analysis aimed at considering PR under a compressive load. Numerical simulations were performed using ANSYS software (ANSYS Inc., Canonsburg, PA, USA). To better evaluate single-cell behavior, a simulation model with nine cells in a 3 × 3 arrangement was used (Figure 5). In this model, only the deformation of the central auxetic cell was considered to reduce the effect of the boundary conditions on the simulation results.

The performance of the middle section of the cells was simulated using a 2D element, that is, the plane183 of the ANSYS library consisting of eight or six nodes with two degrees of freedom, which are the translations in the X and Y directions of the node. This element is recommended for irregular meshes where the design is imported from computer-aided design (CAD) software, such as SolidWorks (Dassault Systèmes, Vélizy-Villacoublay, France). The element size of the FEM model was set at 0.25 mm. With this value, the computation time is reduced, and convergence is achieved even when geometric nonlinearity is enabled. The behavior of the flexible TPU material was modeled with an elastic modulus (E) of 20 MPa and Poisson's ratio ν of 0.4, while for the rigid PLA material, the properties were set to $E = 3{,}500$ MPa and $\nu = 0.36$. Two different meshes, one for each material, were generated, and the common nodes were merged to avoid contact conditions on the adjacent sides. The mesh generated for the 3 × 3 elementary cell arrangement, together with the details of the central cell, is shown in Figure 5. This figure highlights the constraints imposed, which have the dual effect of blocking the translation of the lower elements along the Y-axis and restricting the translation along the X-axis only for elements on the extreme right side.

Figure 5 Mesh generated through Ansys software for FEM analysis of a 3 × 3 elementary cell arrangement with a magnification of the central cell

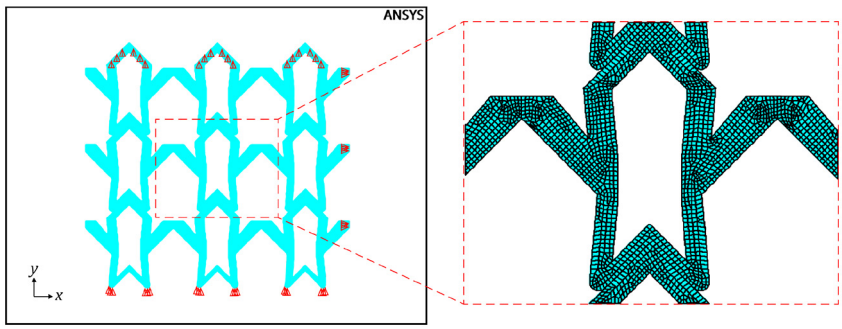

Source: Figure by authors

The structures were compressed along the Y-axis, and the S displacement of a node of the central element was calculated to determine the fictitious PR ν_f and to compare the two configurations. Figure 6 shows the deformations of the cells from the starting position, which is represented in a wireframe graphic with contours, to the final arrangement, represented by the blue solid shapes. From this figure, it is possible to qualitatively appreciate the auxetic behavior of both configurations that undergo a contraction along the X-axis because of compression along the Y-direction.

Auxetic behavior was quantitatively assessed by calculating cell displacements. In configuration 1 [Figure 6(a)], for a compressive strain of the entire structure of 1 mm along the Y direction, the central element is subjected to a displacement of 0.11 mm (s_x) along the X axis and of 0.61 mm (s_y) along the Y axis. Thus, a fictitious Poisson's ratio ν_f can be calculated as:

$$\nu_f = -\frac{s_x}{s_y} = -\frac{0.11\ mm}{0.61\ mm} = -0.18$$

For configuration 2 [Figure 6(b)], for a compressive strain of the entire structure of 1 mm along the Y direction, the central element is subjected to a displacement of 0.47 mm (s_x) along the X axis and of 0.87 mm (s_y) along the Y axis. Thus, the resulting fictitious Poisson's ratio ν_f is:

$$\nu_f = -\frac{s_x}{s_y} = -\frac{0.47\ mm}{0.87\ mm} = -0.52$$

The latter configuration obtained a Poisson's ratio ν_f three times greater than the former, which is proportional to the increase in angle θ. It can be concluded that by varying the parameters of the NPR structure, a broad range of mechanical performance can be obtained for the same materials. This auxetic behavior is in good accordance with the results reported in the literature (Kumar *et al.*, 2022).

It would be interesting to investigate the development of parametric design modeling to have a deeper understanding and prediction of deformation as a function of θ angle, as reported in previous literature (Mazurkiewicz *et al.*, 2021). Nevertheless, in this initial feasibility study, it was decided not to proceed in the direction of fine optimization of the cell geometry. Thus, the value of the θ angle was not further increased to maintain sufficient distance between the reentrant sides. This choice prevented the inner middle joints [Figure 4(b)] from making contact too early when the structure is loaded because this condition would limit the maximum auxetic contraction. Therefore, configuration 2 is assumed to have an optimal balance between the auxetic properties, geometric packing effect and feasibility.

2.3 3D printing of auxetic jounce bumpers

Starting from the optimized geometry of configuration 2, the jounce bumper was designed in the final form of a single module comprising multiple cells located along a ring (Figure 7). The 25 mm inner radius of the module is larger than that of the

Figure 6 Effect of structural parameters on the mechanical behavior of bidimensional NPR structures for configuration 1 (a) and configuration 2 (b)

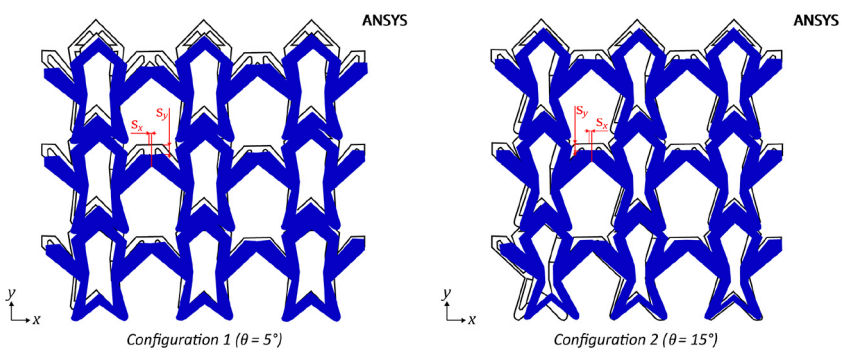

Source: Figure by authors

Figure 7 Single jounce bumper module in the ring shape derived from the single cell of configuration 2

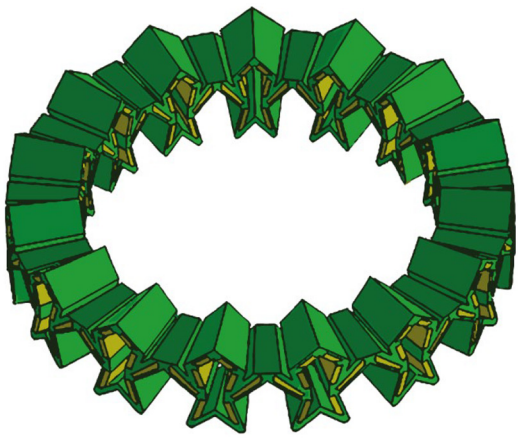

Source: Figure by authors

strut boot, whereas the 70 mm outer diameter of the ring is smaller than that of the shock absorber strut.

All prototypes were fabricated by FFF using an A4v3 [Figure 8(a)] 3D printer (3ntr, Oleggio, Italy) with three extruders: one for the flexible green TPU material, one for the rigid yellow PLA, and the last extruder for the support material was not used. The commercial name of TPU was "ELASTO 85." Similar to the PLA material, it was purchased from 3ntr company (3ntr, Oleggio, Italy). Table 1 lists the primary material properties extracted from the datasheet provided by the supplier. These values were used in the subsequent numerical simulations. The same table also summarizes the 3D printing parameters used. Although the final properties of 3D-printed samples will depend strongly on the printing direction (Kucewicz *et al.*, 2019; Kucewicz *et al.*, 2019), the printing direction of the test parts was chosen to avoid the use of supports.

To better distribute the compression load on the auxetic ring module, flat surfaces for contact with the crossheads of the testing machine were introduced by modifying the design shown in Figure 7. In fact, the contact of a single line with a plane would not ensure a uniaxial compressive action in the vertical direction because it would also involve lateral components of the force, leading to instability and sliding. Therefore, two bases were added at the bottom joints (green dots) of the cell in Figure 4(b), whereas the top sharp joint was removed by

Table 1 Material properties from datasheet and 3D printing parameters

Properties	PLA	TPU
Young's modulus [MPa]	3,200	44
Yield tensile strength [MPa]	53	4.3
Elongation at yield [%]	6	46.1
Compression modulus [MPa]	N.a.	38
Melting temperature [°C]	135	168
Glass transition temperature [°C]	55	−35
Density [g/cm^3]	1.24	1.19
Hardness	N.a.	85 Shore A
Printing parameters		
Extruder temperature [°C]	195	210
Bed temperature [°C]	60	60
Printing speed [mm/s]	15	20
Layer height [mm]	0.2	0.2
Extrusion width [mm]	0.4	0.4
Infill pattern	Rectilinear	Rectilinear
Infill percentage [%]	100	100

Note: N.a. stands for "not available"
Source: Table by authors

extending the sharp triangular shape to a small top plane of approximately 4 mm in width. The resulting geometry of the modified auxetic cell and ring module is shown in Figure 8(b) for the 3D printed jounce bumper with a height of about 15 mm, similar to the original cell in Figure 4(a).

Moreover, to assess whether the creation of a single module or a configuration with multiple modules affected the compression tests, an additional prototype was created. This prototype consisted of a double module of the auxetic cell ring printed as one piece with a total height of approximately 27.5 mm [Figure 8(c)]. The auxetic cells of the lower module of this one-piece ring have the original design derived from configuration 2, with the top sharp edge to properly match the triangular base of the cells of the upper module.

With the parameters in Table 1, the single module of the jounce bumper was printed in about 3 h, whereas it took almost 6 h to print the double one-piece module. Both prototypes were affected by the stringing defect, as small, thin strings of the TPU material [Figure 8(b) and 8(c)] were left behind by the nozzle during printing.

To evaluate the 3D printing accuracy and reproducibility of the single auxetic cell, the real geometry of the 3D printed single module of the NPR jounce bumper in the modified ring shape [Figure 8(b)] was obtained through X-ray Computed

Figure 8 Photo of the FFF printer A4v3 by 3ntr (a); 3D printed single module of the NPR jounce bumper in the modified ring shape (b) and the double one-piece module of the NPR jounce bumper (c)

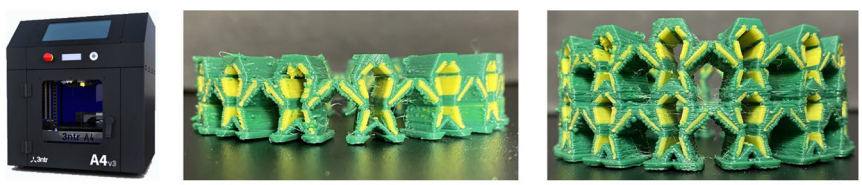

(a) **(b)** **(c)**

Source: Figure by authors

Tomography (X-CT) using a Phoenix v|tome|x S240 (GE Baker Hughes – Waygate Technologies, Wunstorf, Germany). A voxel size of 74 μm was used to perform the X-CT scan, and the source was supplied with a voltage of 220 kV and a current of 200 μA to acquire 1,000 images with a timing of 100 ms. The reconstruction of the X-ray images into a 3D model was performed using datos|reconstruction software (GE Baker Hughes – Waygate Technologies, Wunstorf, Germany), and VG Studio Max software (version 3.4) by Volume Graphics (Hexagon Metrology-Volume Graphics, Heidelberg, Germany) was used for the surface determination using an *Isovalue*-based approach. Based on the surface determination results, the CT-scan data were exported in the STL format for deviation analysis using GOM Inspect Professional software (GOM GmbH, Braunschweig, Germany) version 2022. The real geometry of the ring was aligned and compared with that of the original CAD model. The alignment between the STL model and the nominal CAD reference was performed by a *best fitting* operation with a final residual deviation of 0.23 mm of the pre-alignment algorithm of GOM Inspect software. The comparison of the STL model for the full ring was computed by GOM Inspect for 2,013,578 data points and provided a mean distance of −0.04 mm with a standard deviation of 0.51 mm from the nominal CAD geometry (Figure 9). The deviation analysis was limited to a search distance of ±2 mm, as points or areas with higher deviation were assumed to be singular printing defects in the deposition of the two materials by the 3ntr extrusion head.

The dimensional deviation analysis conducted on the entire ring also included cumulative errors in the printing of single cells distributed along the circular arrangement. Therefore, to evaluate the reproducibility of the 3D printing process on a single auxetic element, a dimensional analysis was repeated for each individual cell. For this purpose, the STL data of every single cell were isolated and extracted from the CT scan data of a full ring consisting of 15 cells.

Reproducibility analysis was then performed using the GOM Inspect software, following the same procedure used for the entire ring module. After the *best-fit* alignment, the STL data of the single cells were compared with the CAD geometry of the auxetic cell. The results of the analyses for the 15 different cells are reported in Table 2, and the chromatic deviation map of the single eighth cell is shown in Figure 10 as an example for all single auxetic elements.

This figure provides evidence of the correspondence between the real part [Figure 10(a)] and the deviations of the same part [Figure 10(b)] from the ideal CAD model calculated from the scan data. The printed parts show larger deviations and the worst definition of cell geometry, especially at the start and end points of the material change, as well as on the downward surfaces. These surfaces were tilted at an angle equal to or larger than 45° to the build direction, with the aim of printing them without the use of supports. However, this case, as many others, shows that the support structures are suggested and useful for improving the aesthetics and finish of downward surfaces.

Reproducibility analysis results in Table 2 show that the mean deviation of cell geometry ranges from −0.09 mm to 0.06 mm, while the standard deviation varies in the range between 0.24 mm and 0.51 mm. Considering the residual deviation of the *best-fit* alignment, it can be stated that the 3D printing process can reproduce the geometry of a single auxetic cell with high accuracy. Conversely, the arrangement of the single modules in the modified ring shape (Figure 9) differs more significantly from that of the nominal CAD model

Figure 9 Chromatic map of dimensional deviation of the 3D printed single module in the modified ring shape CT scan compared with the nominal CAD model

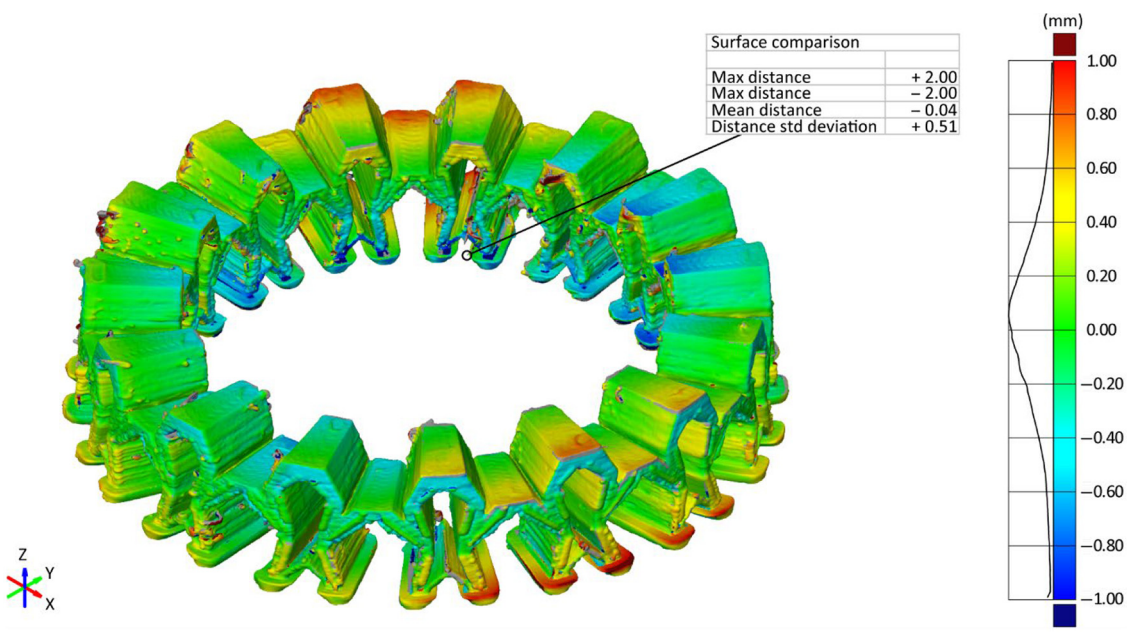

Source: Figure by authors

Table 2 Dimensional analyses of the 3D printed single cells compared with the nominal CAD model

Cell	*Best fit* deviation [mm]	Data points [adm]	Mean deviation [mm]	Standard deviation [mm]
1	0.08	121,869	0.03	0.34
2	0.10	125,458	0.03	0.36
3	0.11	125,972	0.06	0.36
4	0.11	125,311	0.04	0.33
5	0.07	114,590	0.04	0.24
6	0.07	135,717	−0.05	0.44
7	0.08	128,578	−0.06	0.39
8	0.07	129,383	−0.05	0.40
9	0.08	117,177	−0.02	0.31
10	0.08	121,690	−0.03	0.32
11	0.10	128,567	−0.06	0.37
12	0.10	124,555	−0.06	0.40
13	0.11	132,073	−0.08	0.45
14	0.10	149,146	−0.09	0.51
15	0.11	145,485	−0.06	0.46
Average values	0.09	128,371	−0.02	0.38

Source: Table by authors

Figure 10 Chromatic map of dimensional deviation of the 3D printed single eighth auxetic cell CT scan compared with the nominal CAD model

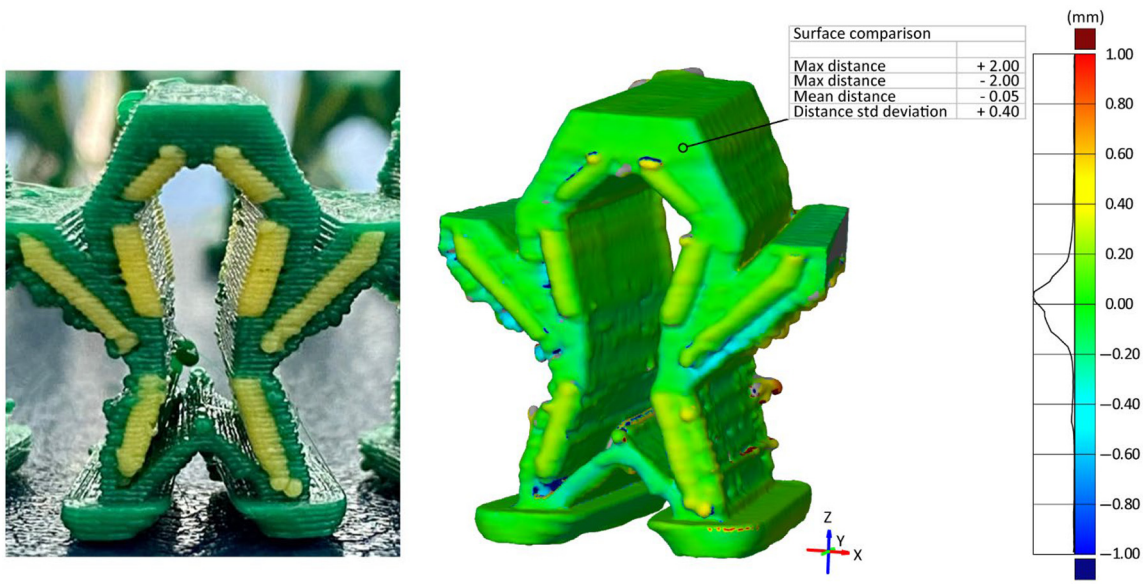

(a) (b)

Source: Figure by authors

because of the constraints and deformations imposed by the neighboring cells in the circular configuration.

3. Compression tests and results

3.1 Experimental results for single module jounce bumpers

To evaluate the performance of the 3D-printed NPR jounce bumpers and conduct a comparison with previous studies in the literature, compression tests were performed using an Aura 5T machine (Easydur, Arcisate, Italy). The first compression test of the single-module NPR jounce bumper was carried out at a speed of 3 mm/min, which is different from the speed of 50 mm/min proposed by the guidelines (Wang *et al.*, 2016a, 2016b). However, the test was replicated at 50 mm/min to compare the results and evaluate the influence of the strain rate [Figure 11(a)].

The use of numerical simulation as a method to mimic the behavior of a multimaterial jounce bumper for design purposes was also investigated. To limit the computational time, the

Figure 11 Effect of the compressive test rate and comparison with simulation result (a); FEM mesh of the single auxetic cell for numerical simulation of the compression test (b)

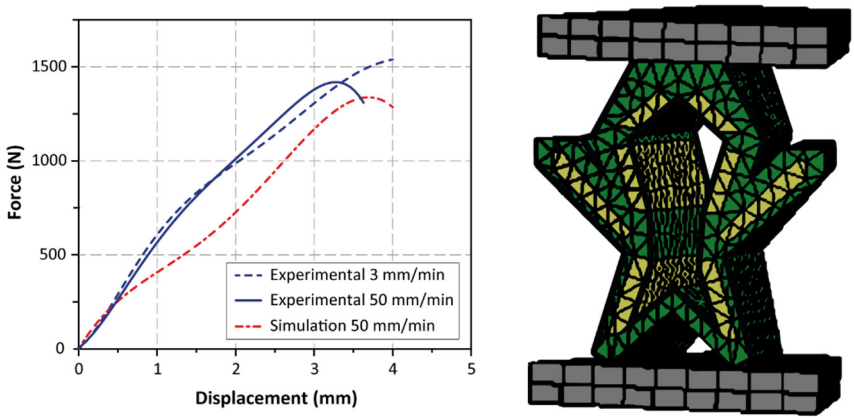

Source: Figure by authors

axial symmetry of the auxetic ring module was exploited, and only a single cell [Figure 11(b)] was modeled in the numerical analysis.

The simulation explicitly promoted convergence owing to the type of phenomenon studied. In the numerical simulation, a rigid contact condition was imposed on the nodes of the lower and upper surfaces of the cell in contact with the lower and upper plates, respectively. The lower plate was constrained and fixed, while a vertical displacement of 5 mm was imposed on the upper plate. A test duration of 6 s was set to achieve a moving speed of the top crosshead of 50 mm/min, as required by the guidelines (Wang *et al.*, 2016a, 2016b) for the compression test. To reduce the simulation time, a discretization with tetragonal elements having a minimum size of 0.2 mm was chosen. With these parameters, the simulation lasted 3 h, and the results were compared to the experimental ones in Figure 11(a).

The divergence between the experimental and simulated curves can be attributed to the constraints imposed to simulate axial symmetry and mesh quality. However, it can be concluded that the numerical results approximate the experimental results satisfactorily. Thus, the simulation approach can be used in the initial design of the jounce bumpers to predict the real behavior of new NPR structures.

Furthermore, from the graph in Figure 11(a), it can be concluded that the higher testing speed did not lead to substantial changes in the behavior of the component, except for a partial delay in the response when the applied load increases at about 3.5 mm of displacement. Consequently, it can be assumed that the test results were not dependent on the compression speed for the examined rates. Therefore, all subsequent compression tests were performed at a speed of 3 mm/min to better monitor the deformation of the 3D-printed jounce bumpers.

3.2 Experimental results for multiple module jounce bumpers

Because of some unsuccessful prints, it was decided not to produce multiple-module jounce bumpers as one piece apart from the double-module one [Figure 8(c)]. However, to increase the height of the jounce bumper, a total of four single-module NPR rings were 3D printed [Figure 12(a)].

The production took approximately 6 h for each ring but avoided material waste in the case of aborted prints for the one-piece four-module ring, whose production would have required more than 15 h. Except for the first prototype [Figure 8(b)], all

Figure 12 3D printed replicas of the single-module NPR jounce bumper (a); four stacked modules of the NPR ring (b)

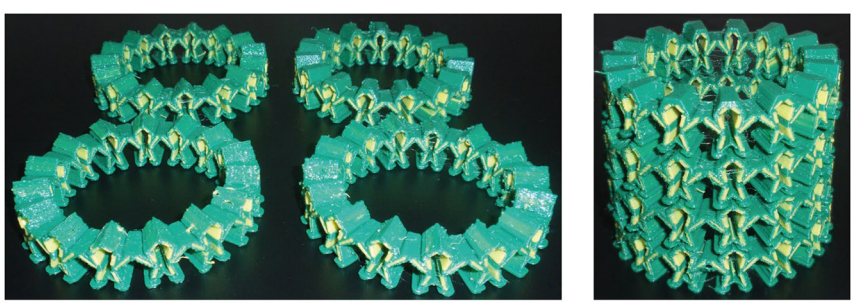

Source: Figure by authors

other replicas of the single-module ring in Figure 12 were printed with the sharp top triangular edge of Figure 7. Sharp-edge replicas were used as bottom or intermediate modules when stacking multiple modules one on top of the other to increase the total height of the NPR jounce bumper. The first prototype, with a flat top surface, was always placed on the top of the stack for better contact with the crosshead of the testing machine [Figure 12(b)].

Compression tests [Figure 13(a)] were performed for two (long dashed line) and four stacked modules (two-dash line), and the test results were compared to those of the single module (dotted line) and the double one-piece module (solid line) NPR rings.

From Figure 13(a), it can be observed that the stiffness of the jounce bumper decreases as the number of stacked modules increases. In fact, the slope of the curve of the four stacked modules (two-dash line) is lower than that of the curve of the two stacked modules (long dash line). This result was caused by the improper packaging of the stacked structures and auxetic cells under the compressive load [Figure 13(b)]. This outcome is probably due to a relative side motion and sliding between the single modules that lie on the top of each other. The same phenomenon was not observed in the compression test of the double one-piece NRP ring (solid line), which had the highest stiffness. Therefore, the physical justification for the large variability in the response between configurations lies mainly in the effect of relative packing and slippage between modules, which is noticeably accentuated in the case of the stacked configurations rather than the single piece. To compare the results, the displacements of the different tested configurations were considered for a compressive load of 450 N [red horizontal line in Figure 13(a)]. The deformation for the single ring (dotted line) of auxetic cells is about 1.25 mm and is almost 54% higher than the one of the double one-piece module (solid line), which is 0.81 mm. For the same load, the displacement of the two stacked NPR modules (long dashed line) was approximately 4.39 mm, whereas the four stacked modules (two-dash line) deformed by 11.7 mm because of an evident collapse of the stack [Figure 13(b)].

Another important aspect to consider is the total elastic energy, which can be stored in different configurations. As previously presented in the literature (Płatek *et al.*, 2020), this is a key parameter for a final application, such as automotive suspension. The data plotted in Figure 13(a) were analyzed, and the different areas subtended by the curves in the elastic region were calculated, representing the total stored energy E_{TOT} up to their elastic limit. The results are presented in Table 3. The total elastic energy reaches the maximum value for the four-stacked module (two-dash line). However, it must be considered that this finding is strongly affected by the greater height of the component. In fact, when considering the energy E_2 stored in the first 2 mm of the displacement, the maximum is found for the double one-piece module (solid line).

These results clearly indicate that the optimal choice is to print multiple-module jounce bumpers as a single piece, avoiding stacking single modules. However, 3D printing issues should first be solved for successful extrusion of a combination of rigid and flexible materials without support structures for sustainability purposes.

The results obtained in this study cannot be directly compared with those of similar 3D-printed components in the literature. Wang *et al.* developed a component with a height of nearly 70 mm by applying the PolyJet technology (Wang *et al.*, 2016a, 2016b), which deposits photopolymer resins onto the printing platform and cures them in place by irradiation with a UV lamp. The PolyJet device underwent axial deformation of up to 20 mm before collapse. Since our study is a preliminary investigation, we did not obtain a component with a height extension comparable to the reference, and thus a load–displacement curve up to 20 mm of movement could not be obtained.

However, for small deformations, the double one-piece module (solid line) NPR ring in this study can be compared to a conventional jounce bumper as a reference, and stiffer behavior

Figure 13 Compression tests of multiple module NPR rings (a); image of the collapsing structure during the compression test of four-stacked NPR modules (b)

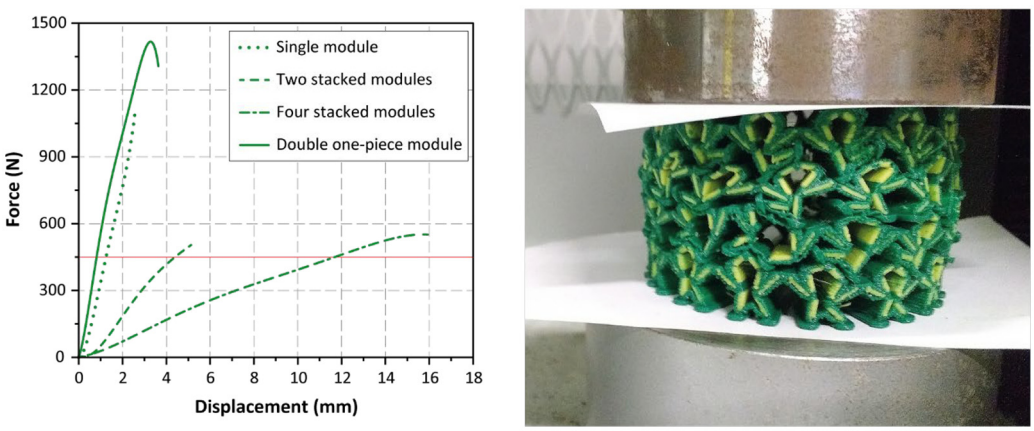

(a) (b)

Source: Figure by authors

Table 3 Elastic energy stored for different configurations of the NPR ring

	Single module	Two-stacked module	Four-stacked module	Double one-piece module
E_{TOT} [J]	1.27	1.28	3.77	1.97
E_2 [J]	0.77	0.19	0.07	1.01

Source: Table by authors

can be observed. A displacement of 3 mm was obtained for a compression load of approximately 1,380 N [solid line in Figure 13(a)], whereas a traditional system deformed up to about 25 mm at the same load (Wang *et al.*, 2016a, 2016b).

3.3 Repeatability analysis

Additional compression tests were carried out to complete this study and to evaluate how the repeatability of 3D printing may affect the variability of the jounce bumper behavior. To this end, four additional replicas of a single-module NPR ring with a flat top surface [Figure 8(b)] were produced using the A4v3 printer.

The poor consistency of the compression test results for the four samples is shown by the load–displacement curves in Figure 14. Two different trends can be observed: sample 1 (solid line) and sample 4 (long dashed line) had a stiffer behavior. They underwent a displacement of approximately 2.5 mm for an applied load of about 1,000 N. Conversely, samples 2 (dotted line) and 3 (dotdash line) underwent a deformation of approximately 5 mm, which is twice the value of previous specimens for the same load. At this specific load of 1,000 N, a maximum displacement variance of approximately 2.5 mm among all samples was observed. There was also a significant difference in the maximum compression force withstood by the four specimens. In fact, both samples 2 (dotted line) and 3 (dotdash line) reached a maximum load of about 1,000 N, which is approximately one third lower than the load of sample 1 (solid line) and almost half the value of the load of sample 4 (long dashed line), i.e. 1,850 N. Since there was no variation in the geometry or printing parameters of the samples, these different results can be ascribed to the inaccuracies and defects in the 3D printing process. Beyond the printing defects visible in Figure 10, a lack of bonding and scarce adhesion at the interfaces between the TPU and PLA materials may emerge when the samples are loaded, and their resistance is tested. Thus, it can be reasonably asserted that the quality of the AM process significantly affects the performance of the final components.

Figure 14 Compression curves of single module NPR rings for repeatability analysis

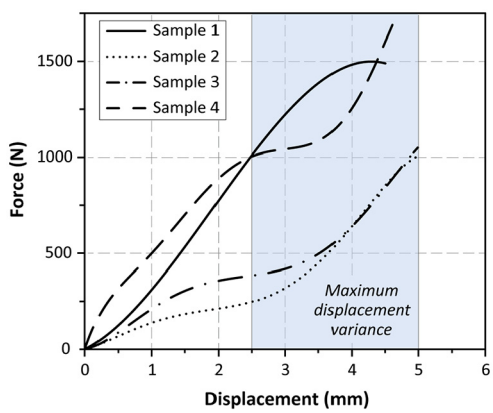

Source: Figure by authors

In general, materials that might be the most appropriate for automotive suspension applications are energy-dissipating ones, which can absorb shock and thus have high resilience. Thermoplastic elastomers and the thermoplastic polyurethanes (TPU) are among the most interesting materials. It would be useful to investigate the impact of the hardness of different grades of TPU. For example, using a harder grade of TPU, such as the "ELASTO 95," with 95 points of Shore A hardness, the auxetic cell can be printed with the flexible material only. Therefore, the removal of PLA as a co-printing material could eliminate the junction points, which are stress concentrators at the PLA–TPU interface inter- and intra-layers, thus improving the repeatability of the results.

4. Conclusions

In this study, different modules of a multimaterial jounce bumper with auxetic properties were fabricated using FFF. The advantage of this auxetic structure, combining flexible TPU and rigid PLA materials, lies in the possibility of lateral shrinkage under compression, with an improvement in the stiffness of the entire component. Simulative and experimental approaches were combined to characterize the specimens. The main findings showed that multiple-module auxetic jounce bumpers printed as a single-piece assembly are stiffer and experience smaller compression strokes than stacked modules under the same load. However, owing to the variability in the quality of 3D-printed specimens, the experimental compression results showed poor repeatability for the maximum load or maximum displacement values.

Therefore, further investigations are required to improve the quality of 3D-printed multimaterial jounce bumpers with the goal of better repeatability of the auxetic structure behavior. To this end, in the future development of this work, an important target will be to improve the inaccuracies described above, for example, by using a smaller extruder nozzle or 0.1 mm layer height. In addition, the PLA material could be substituted by another polymer, such as high impact-resistant polystyrene, to enhance the adhesion with the flexible TPU envelope.

This study opened new frontiers for an attractive application of AM in the automotive sector. Indeed, a multimaterial jounce bumper with auxetic properties that can effectively reduce NVH by absorbing impact energy is a crucial component of the vehicle suspension system. The proposed final solution is innovative because, for the first time, a multimaterial NPR jounce bumper was manufactured in a single production step without the need to assemble or glue individual parts. In

addition, the exploited auxetic geometry and printing direction did not require support structures. From a sustainability and manufacturing perspective, all these aspects imply considerable higher efficiency, which would be worth evaluating with a life cycle assessment.

Future research should further investigate the characterization of 3D-printed jounce bumpers by evaluating their fatigue-end endurance and the influence of strain rate. However, these activities are beyond the scope of this preliminary study and represent a valuable outlook for future development.

References

Alderson, A. and Alderson, K.L. (2007), "Auxetic materials", *Proceedings of the Institution of Mechanical Engineers, Part G: Journal of Aerospace Engineering*, Vol. 221 No. 4, pp. 565-575, doi: 10.1243/09544100JAERO185.

Alderson, K.L., Alderson, A., Smart, G., Simkins, V.R. and Davies, P.J. (2002), "Auxetic polypropylene fibres: part 1 – manufacture and characterisation", *Plastics, Rubber and Composites*, Vol. 31 No. 8, pp. 344-349, doi: 10.1179/146580102225006495.

Baughman, R.H. and Galvão, D.S. (1993), "Crystalline networks with unusual predicted mechanical and thermal properties", *Nature*, Vol. 365 No. 6448, pp. 735-737, doi: 10.1038/365735a0.

Baughman, R.H., Galvao, D.S., Cui, C. and Dantas, S.O. (1997), "Hinged and chiral polydiacetylene carbon crystals", *Chemical Physics Letters*, Vol. 269 Nos 3/4, pp. 356-364.

Chapa, A., Cuan-Urquizo, E., Urbina-Coronado, P. and Roman-Flores, A. (2023), "Experimental characterization of the mechanical properties of 3D printed TPU auxetic cellular materials under cyclic compressive loadings", *Rapid Prototyping Journal*, doi: 10.1108/RPJ-07-2022-0226.

Friis, E.A., Lakes, R.S. and Park, J.B. (1988), "Negative poisson's ratio polymeric and metallic foams", *Journal of Materials Science*, Vol. 23 No. 12, pp. 4406-4414, doi: 10.1007/BF00551939.

Guo, C., Zhao, D., Liu, Z., Ding, Q., Gao, H., Yan, Q., Sun, Y., *et al.* (2021), "The 3D-printed honeycomb metamaterials tubes with tunable negative poisson's ratio for high-performance static and dynamic mechanical properties", *Materials, MDPI AG*, Vol. 14 No. 6, doi: 10.3390/ma14061353.

Han, Y. and Lu, W. (2018), "Evolutionary design of nonuniform cellular structures with optimized poisson's ratio distribution", *Materials and Design, Elsevier Ltd*, Vol. 141, pp. 384-394, doi: 10.1016/j.matdes.2017.12.047.

Hedayati, R., Güven, A. and van der Zwaag, S. (2021), "3D gradient auxetic soft mechanical metamaterials fabricated by additive manufacturing", *Applied Physics Letters*, Vol. 118 No. 14, p. 141904, doi: 10.1063/5.0043286.

Herakovich, C.T. (1984), "Composite laminates with negative through-the-thickness poisson's ratios", *Journal of Composite Materials*, Vol. 18 No. 5, pp. 447-455.

Hu, H., Gan, L. and Huang, J. (2022), "Facile and universal method to obtain negative poisson's ratio via support-free 3D printing tetrahedron-framework", *Advanced Engineering Materials*, Vol. 24 No. 7, p. 2101359, doi: 10.1002/ADEM.202101359.

Jiang, Y. and Li, Y. (2017), "3D printed chiral cellular solids with amplified auxetic effects due to elevated internal rotation", *Advanced Engineering Materials*, Vol. 19 No. 2, doi: 10.1002/adem.201600609.

Jiang, W., Ren, X., Wang, S.L., Zhang, X.G., Zhang, X.Y., Luo, C., Xie, Y.M., *et al.* (2022), "Manufacturing, characteristics and applications of auxetic foams: a state-of-the-art review", *Composites Part B: Engineering*, Vol. 235, p. 109733, doi: 10.1016/J.COMPOSITESB.2022.109733.

Joseph, A., Mahesh, V. and Harursampath, D. (2023), "On the application of additive manufacturing methods for auxetic structures: a review", *Advances in Manufacturing*, Vol. 9 No. 3, doi: 10.1007/s40436-021-00357-y.

Kucewicz, M., Baranowski, P. and Małachowski, J. (2019), "A method of failure modeling for 3D printed cellular structures", *Materials & Design*, Vol. 174, doi: 10.1016/j.matdes.2019.107802.

Kucewicz, M., Baranowski, P., Stankiewicz, M., Konarzewski, M., Płatek, P. and Małachowski, J. (2019), "Modelling and testing of 3D printed cellular structures under quasi-static and dynamic conditions", *Thin-Walled Structures*, Vol. 145, doi: 10.1016/j.tws.2019.106385.

Kumar, S., Vyavahare, S., Teraiya, S., Kootikuppala, J. and Bogala, H. (2022), "A state of the art review of additively manufactured auxetic structures", in Dave Harshit K. and Dixit, U.S. and N.D. (Eds), *Recent Advances in Manufacturing Processes and Systems*, Springer Singapore, Singapore, pp. 69-84.

Lu, Z.X., Li, X., Yang, Z.Y. and Xie, F. (2016), "Novel structure with negative Poisson's ratio and enhanced Young's modulus", *Composite Structures*, Vol. 138, pp. 243-252, doi: 10.1016/j.compstruct.2015.11.036.

Mazurkiewicz, ŁA., Bukała, J., Małachowski, J., Tomaszewski, M. and Buszman, P.P. (2021), "BVS stent optimisation based on a parametric model with a multistage validation process", *Materials & Design*, Vol. 198, doi: 10.1016/j.matdes.2020.109363.

Meena, P., Calius, S. and Singamneni, K.E. (2023), "An enhanced square-grid structure for additive manufacturing and improved auxetic responses", *International Journal of Mechanics and Materials in Design*, Vol. 15 No. 2, doi: 10.1007/s10999-018-9423-8.

Meena, K. and Singamneni, S. (2021), "Novel hybrid auxetic structures for improved in-plane mechanical properties via additive manufacturing", *Mechanics of Materials, Elsevier B.V*, Vol. 158, doi: 10.1016/J.MECHMAT.2021.103890.

Płatek, P., Rajkowski, K., Cieplak, K., Sarzyński, M., Małachowski, J., Woźniak, R. and Janiszewski, J. (2020), "Deformation process of 3D printed structures made from flexible material with different values of relative density", *Polymers*, Vol. 12 No. 9, doi: 10.3390/POLYM12092120.

Ramírez-Gutiérrez, D.L., Cuan-Urquizo, E. and Fuentes-Aguilar, R.Q. (2023), "Sine-based lattice plates: additive manufacturing and their mechanical properties when loaded out of plane", *Rapid Prototyping Journal*, doi: 10.1108/RPJ-01-2023-0010.

Wang, Y., Ma, Z.-D. and Wang, L. (2016a), "A finite element stratification method for a polyurethane jounce bumper", *Proc IMechE Part D: J Automobile Engineering*, Vol. 230 No. 7, pp. 983-992, doi: 10.1177/0954407015602578.

Wang, Y., Wang, L., Ma, Z.-D. and Wang, T. (2017), "Finite element analysis of a jounce bumper with negative poisson's ratio structure", *Journal of Mechanical Engineering Science*, Vol. 231 No. 23, pp. 4374-4387, doi: 10.1177/0954406216665415.

Wang, Y., Wang, L., Ma, Z.D. and Wang, T. (2016b), "A negative poisson's ratio suspension jounce bumper", *Materials & Design*, Vol. 103, pp. 90-99, doi: 10.1016/j.matdes.2016.04.041.

Wang, Y., Wanzhong, Z., Guan, Z., Wang, C. and Qiang, G. (2018c), "Parametric design strategy of a novel cylindrical negative poisson's ratio jounce bumper for ideal uniaxial compression load-displacement curve", *Science China Technological Sciences*, Vol. Vol. 61 No. 10, pp. 1611-1620, doi: 10.1007/s11431-017-9194-2.

Wang, Y., Zhao, W., Zhou, G., Gao, Q. and Wang, C. (2018a), "Optimization of an auxetic jounce bumper based on Gaussian process metamodel and series hybrid GA-SQP algorithm", *Structural and Multidisciplinary Optimization*, Vol. 57 No. 6, pp. 2515-2525, doi: 10.1007/s00158-017-1869-z.

Wang, Y., Zhao, W., Zhou, G., Gao, Q. and Wang, C. (2018b), "Suspension mechanical performance and vehicle ride comfort applying a novel jounce bumper based on negative Poisson's ratio structure", *Advances in Engineering Software*, Vol. 122, pp. 1-12, doi: 10.1016/j.advengsoft.2018.04.001.

Wojciechowski, K.W. (1987), "Constant thermodynamic tension Monte Carlo studies of elastic properties of a two-dimensional system of hard cyclic hexamers", *Molecular Physics*, Vol. 61 No. 5, pp. 1247-1258, doi: 10.1080/00268978700101761.

Zhang, J., Lu, G. and You, Z. (2020), "Large deformation and energy absorption of additively manufactured auxetic materials and structures: a review", *Composites Part B: Engineering*, Vol. 201, doi: 10.1016/j.compositesb.2020.108340. Elsevier Ltd, 15 November.

Corresponding author

Alberto Giubilini can be contacted at: alberto.giubilini@polito.it